Polyhydrido Copper Nanoclusters with a Hollow Icosahedral Core [Cu30H18E2P(OR)212] (E = S or Se; R = n Pr, i Pr or i Bu)

Subrat Kumar Barik, Shou-Chih Huo, Chun-Yen Wu, Tzu-Hao Chiu, Jian-Hong Liao, Xiaoping Wang, Samia Kahlal, Jean-Yves Saillard, Chen-Wei Liu

RESEARCH ARTICLE WILEY-VCH

Polyhydrido Copper Nanoclusters with a Hollow Icosahedral Core: $[Cu_{30}H_{18}\{E_2P(OR)_2\}_{12}]$ (E = S or Se; R = ^{n}Pr, ^{i}Pr or ^{i}Bu)

Subrat Kumar Barik,[#[a]] Shou-Chih Huo, [#[a]] Chun-Yen Wu,[[a]] Tzu-Hao Chiu,[[a]] Jian-Hong Liao, [[a]] Xiaoping Wang,[[b]] Samia Kahlal,[[c]] Jean-Yves Saillard,*[[c]] and C. W. Liu *[[a]]

Dedicated to our colleague and friend Dr. Jean-Rene Hamon on the occasion of his 65th birthday

Abstract: Although atomically precise polyhydrido copper nanoclusters are of prime interest for a variety of applications, they have so far remained scarce. Herein, we describe the synthesis of a dithiophosphate-protected copper(I) hydride-rich nanocluster (NC), $[Cu_{30}H_{18}\{S_2P(O^nPr)_2\}_{12}]$ (**1_H**), fully characterized by various spectroscopic methods and single crystal X-ray diffraction. The X-ray structure of **1_H** reveals an unprecedented central Cu_{12} hollow icosahedron. Six faces of this icosahedron are capped by Cu_3 triangles, the whole Cu_{30} core being wrapped by twelve dithiophosphate ligands and the whole cluster has ideal S_6 symmetry. The locations of the 18 hydrides in **1_H** were ascertained by a single crystal neutron diffraction study. They are composed of three types: capping μ_3-H, interstitial μ_4-H (seesaw) and μ_5-H ligands (square pyramidal), in good agreement with the DFT simulations. The numbers of hydrides and ligand resonances in the ^{1}H NMR spectrum of **1_H** are in line with their coordination environment in the solid-state, retaining the S_6 symmetry in solution. Furthermore, two new Se-protected polyhydrido copper nanoclusters, $[Cu_{30}H_{18}\{Se_2P(OR)_2\}_{12}]$ (**2_H:** R = ^{i}Pr **3_H:** R = ^{i}Bu) were synthesized from their sulfur relative **1_H** *via* ligand displacement reaction and their X-ray structures feature the exceptional case where both the NC shape and size are fully conserved during the course of ligand exchange. DFT and TD-DFT calculations allow understanding the bonding and optical properties of clusters **1_H**-**3_H**. In addition, the reaction of **1_H** with $[Pd(PPh_3)_2Cl_2]$ in the presence of terminal alkynes led to the formation of new bimetallic Cu-Pd alloy clusters $[PdCu_{14}H_2\{S_2P(O^nPr)_2\}_6(C{\equiv}CR)_6]$ (**4:** R = Ph; **5:** R **=** C_6H_4F).

Introduction

Since the discovery of the first binary copper hydride in 1844 by Wurtz (hexagonal Wurtzite-type structure),[1,2] several multinuclear copper hydrido and polyhydrido complexes and clusters, protected by various types of ligands (phosphines, pyridines and N-heterocyclic carbenes) were synthesized.[3-14] They have been capturing substantial interest, not only from the viewpoints of their fascinating structural features,[15-17] but also owing to their promising applications as hydrogen storage materials[18-23] and as key intermediates in various catalytic transformations in organic synthesis.[24, 25] An emblematic example is the well characterized phosphine-protected $[CuH(PPh_3)]_6$, widely known as Stryker's reagent, which was shown to be a mild and selective reagent for conjugate reduction of α, β -unsaturated carbonyl compounds.[26] Related chiral phosphine-copper hydride catalysts were employed for the asymmetric hydrosilylation of acetophenone.[27]

In recent years, this copper hydride chemistry has evolved towards the design of nanosized ligand-protected polyhydrido copper clusters which have emerged as a new class of materials in the field of nanoscience, owing to their various potential applications.[15-25, 28-37] Unlike the incredible success found in the chemistry of Au and Ag atomically precise nanoclusters (NCs), that of copper is still in its infancy, which is partly due to the much lower reduction potential of Cu than those of Ag and Au. In this context, only a handful of ligand-supported Cu(0)/Cu(I) mixed-valent polyhydrides have been so far reported,[38-41] and Cu(I) hydrides are merely more numerous.[17,34,42-47] Our recent findings such as $[Cu_{20}(H)_{11}\{E_2P(O^iPr)_2\}_9]$ (E = S,[46] Se[47]), $[Cu_{28}(H)_{15}\{S_2CN(^nPr)_2\}_{12}](PF_6)$,[48] and $[Cu_{32}(H)_{20}\{S_2P(O^iPr)_2\}_{12}]$[49, 50] have not only uncovered fascinating structural architectures (elongated triangular orthobicopula, rhombicuboctahedral and pseudo-rhombohedral core, respectively) but also shown potential applications in solar H_2 evolution. In fact, the latter has been utilized in the electrocatalytic CO_2 reduction via a lattice hydride mechanism and also led to the formation of rhombus-shaped copper nanoparticles upon reduction with excessive amount of $NaBH_4$.[33,49,50] These findings raise the question whether there could exist chalcogen-protected polyhydrido Cu(I) clusters with a hollow icosahedral core framework. Indeed, such a situation has been encountered before in case of Ag and Au clusters.[51,52] The recent discovery of $[Cu_{53}(RCOO)_{10}(C{\equiv}CtBu)_{20}Cl_2H_{18}]^+$ nanocluster by Zheng and co-workers offered the existence of inner $Cu_{10}Cl_2$ empty icosahedron within the four-concentric shell $Cu_3@Cu_{10}Cl_2@Cu_{20}@Cu_{20}$ thus indicated the possibility of empty Cu_{12} icosahedron within a polyhydrido copper NC.[53]

In this article, we report the synthesis and full characterization of a series of 30-metal and 18-hydride dichalcogenolate-protected copper clusters, namely $[Cu_{30}(H)_{18}\{E_2P(O^nR)_2\}_{12}]$ (**1_H** : E = S, R = ^{n}Pr; **2_H:** E = Se, R = ^{i}Pr; **3_H:** E = Se, R = ^{i}Bu). They all feature a hollow Cu_{12} icosahedral core, a structure that has not been characterized before amongst Cu(I) NCs.

Single crystals suitable for a neutron diffraction analysis could be grown so that the precise location of all the hydrides in **1_H** was successfully uncovered. Remarkably, six four-coordinated hydrides out of total 18 exhibited nearly seesaw geometry, where the central hydride bonds to four Cu atoms with a local C_{2v} symmetry, hitherto unknown in metal hydride chemistry. The reaction of **1_H** with $Pd(PPh_3)_2Cl_2$ in the presence of different alkynes as auxiliary ligands leads to the formation of the new

[a] Dr. S. K. Barik, S.-C. Huo, C.-Y. Wu, T.-H. Chiu, J.-H. Liao, Prof. C. W. Liu*
Department of Chemistry, National Dong Hwa University
No. 1, Sec. 2, Da Hsueh Rd. Shoufeng, Hualien 97401 (Taiwan R.O.C.).
E-mail: chenwei@mail.ndhu.edu.tw
Homepage: http://faculty.ndhu.edu.tw/~cwl/index.htm
# denotes equal contribution of authors
[b] Dr. X. Wang
Neutron Scattering Division, Neutron Sciences Directorate, Oak Ridge National Laboratory, Oak Ridge, TN, 37831, USA
[c] Dr. S. Kahlal, Prof. J.-Y. Saillard*
Univ Rennes, CNRS, ISCR-UMR 6226, F-35000 Rennes, France
E-mail: jean-yves.saillard@univ-rennes1.fr
Supporting information for this article is given via a link at the end of the document.

alloy clusters $[PdCu_{14}H_2\{S_2P(O^nPr)_2\}_6(C{\equiv}CR)_6]$ (**4:** R = Ph; **5:** R = C_6H_4F) which exhibit a $[(PdH_2)^{2-}]$-centered icosahedral core.

Results and Discussion

In a typical one pot synthetic method, the treatment of $(NH_4)[S_2P(O^nPr)_2]$ with $[Cu(CH_3CN)_4]PF_6$ in THF resulted in an immediate color change from colorless to yellow. Addition of $NaBH_4$ to the solution at -20 °C resulted in a gradual color change to orange-red. Continuous stirring at low temperature for 4 hours followed by work-up led to the isolation of $[Cu_{30}H_{18}\{S_2P(O^nPr)_2\}_{12}]$, $\mathbf{1_H}$ in 38 % yield (Scheme 1, Figure S1, see supporting information). Cluster $\mathbf{1_H}$ has been fully characterized by a broad spectrum of standard chemical characterization protocols including ESI mass spectrometry, multinuclear NMR spectroscopy, UV-Vis, X-ray crystallography and neutron diffraction study.

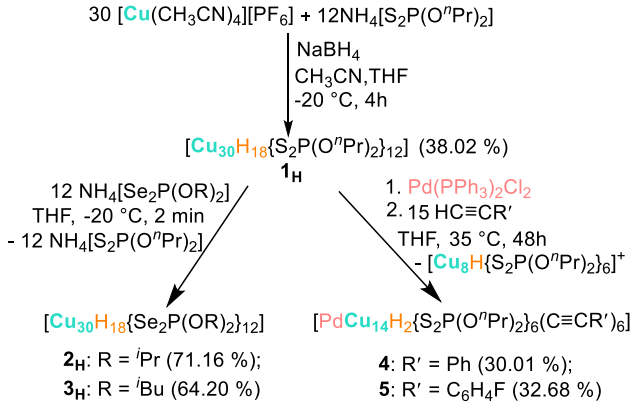

Scheme 1. Synthesis of the dichalogenophosphate protected Cu_{30} NCs ($\mathbf{1_H}$-$\mathbf{3_H}$) and the reactivity of $\mathbf{1_H}$ with Pd^{2+}.

The composition of $\mathbf{1_H}$ was initially obtained by the analysis of its positive-ion ESI-mass spectrum. The spectrum of $\mathbf{1_H}$ evidently shows a most intense peak at *m/z* 4547.3 (calcd. 4547.4), corresponding to $[\mathbf{1_H}+Cu]^+$ and a slightly lower intense peak at *m/z* 4483.4 (calcd. 4483.8), corresponding to molecular weight of neutral $\mathbf{1_H}$ (Figure 1). Their simulated isotopic patterns match well with the experimental observation (Figure 1).

The $^{31}P\{^1H\}$ NMR spectrum of $\mathbf{1_H}$ displays two signals at 112.69 and 108.88 ppm indicating two types of dipropyl dithiophosphate (dtp) ligands in solution at room temperature (Figure S2). ^1H NMR spectrum of $\mathbf{1_H}$ shows three different signals at 4.22-4.05, 1.70, and 0.97 ppm in 1:1:1.5 intensity ratios corresponding to the $-OCH_2$, CH_2, and CH_3 protons, respectively attributed to propyl groups in dtp ligands (Figure 2a, S3). In addition to these propyl peaks, it also shows three broad hydride resonances at 3.52, 0.78, and 0.60 ppm, respectively, in equal intensity (Figure 2a). In order to confirm the presence of hydrides in $\mathbf{1_H}$, its deuteride analogue $[Cu_{30}D_{18}\{S_2P(O^nPr)_2\}_{12}]$ ($\mathbf{1_D}$), was synthesized. The ^2H NMR spectrum of $\mathbf{1_D}$ in $CHCl_3$ shows three broad signals at 3.62, 0.83, and 0.63 ppm with equal intensity (Figure 2b and Figure S4), clearly signifying the existence of three types of hydrides in $\mathbf{1_H}$. Furthermore, the ^1H variable temperature (VT) NMR of $\mathbf{1_H}$ in $CDCl_3$ shows

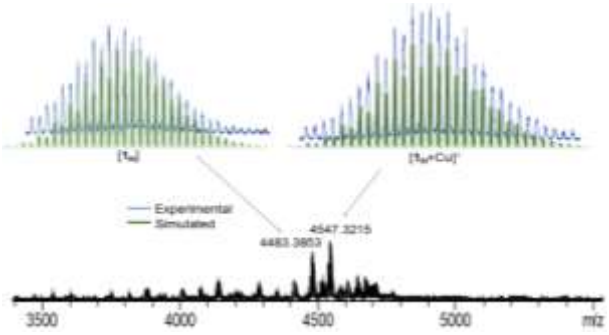

Figure 1. Positive ion ESI-MS of $\mathbf{1_H}$. Insets show experimental (blue) and simulated (green) spectra corresponding to $[\mathbf{1_H}]$ and $[\mathbf{1_H} + Cu]^+$.

the conservation of three hydride signals, indicating the static nature of the molecule in solution (Figure S5). Cluster $\mathbf{1_H}$ is air and moisture stable in solid state at ambient temperature, (Figure S6) while in solution state it is moderately stable at room temperature, losing its identity upon keeping the solution, especially in polar solvents (CH_2Cl_2 and $CHCl_3$), for several days (Figure S7).

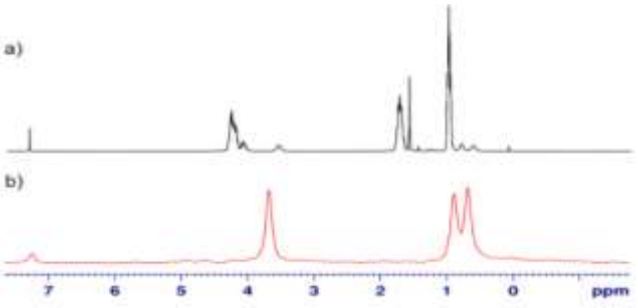

Figure 2. a) ^1H NMR spectrum of cluster $\mathbf{1_H}$ in $CDCl_3$. b) ^2H NMR spectrum of $\mathbf{1_D}$ in $CHCl_3$..

The crystallization of $\mathbf{1_H}$ was performed by vapor diffusion of hexanes into a concentrated CH_2Cl_2 solution at room temperature. Rectangular-shaped red crystals (*P*-1 space group) were obtained within a week. The X-ray diffraction study of compound $\mathbf{1_H}$ revealed a neutrally charged polyhydrido copper NC comprised of 30 copper atoms, 12 dtp ligands, and 18 hydrides (Figure 3a). Shell by shell molecular structure of $\mathbf{1_H}$ can be seen in Figure 3. $\mathbf{1_H}$ features a central core of 12 copper atoms arranged in a non-centered icosahedron, which displays elongation along the C_3 axis (Figure 3c). This Cu_{12} core is connected, via Cu-Cu interactions to six $[Cu_3]$ triangular motifs which cap the icosahedron in an octahedral arrangement (Figure 3d). Hence cluster $\mathbf{1_H}$ possesses ideal S_6 symmetry with the C_3 axis passing through the Cu5-Cu6-Cu15 triangle (Figure 3b and d). Alternatively, the Cu_{30} metal framework in $\mathbf{1_H}$ can be described as an empty Cu_{12} icosahedron embedded in an incomplete rhombicuboctahedral Cu_{18} framework (Figure 3e). Within the Cu_{12} icosahedron, the average Cu_{ico}-Cu_{ico} distance of 2.658 (7) Å (range: 2.504(6)- 2.899(7) Å) is shorter than that observed in the severely distorted Cu_{13} centered icosahedral core in $[Cu_{25}H_{22}(PPh_3)_{12}]Cl$[38] (avg. 2.777 Å, range: 2.470(3)-3.256(3) Å). It is actually closer to that observed for bulk copper

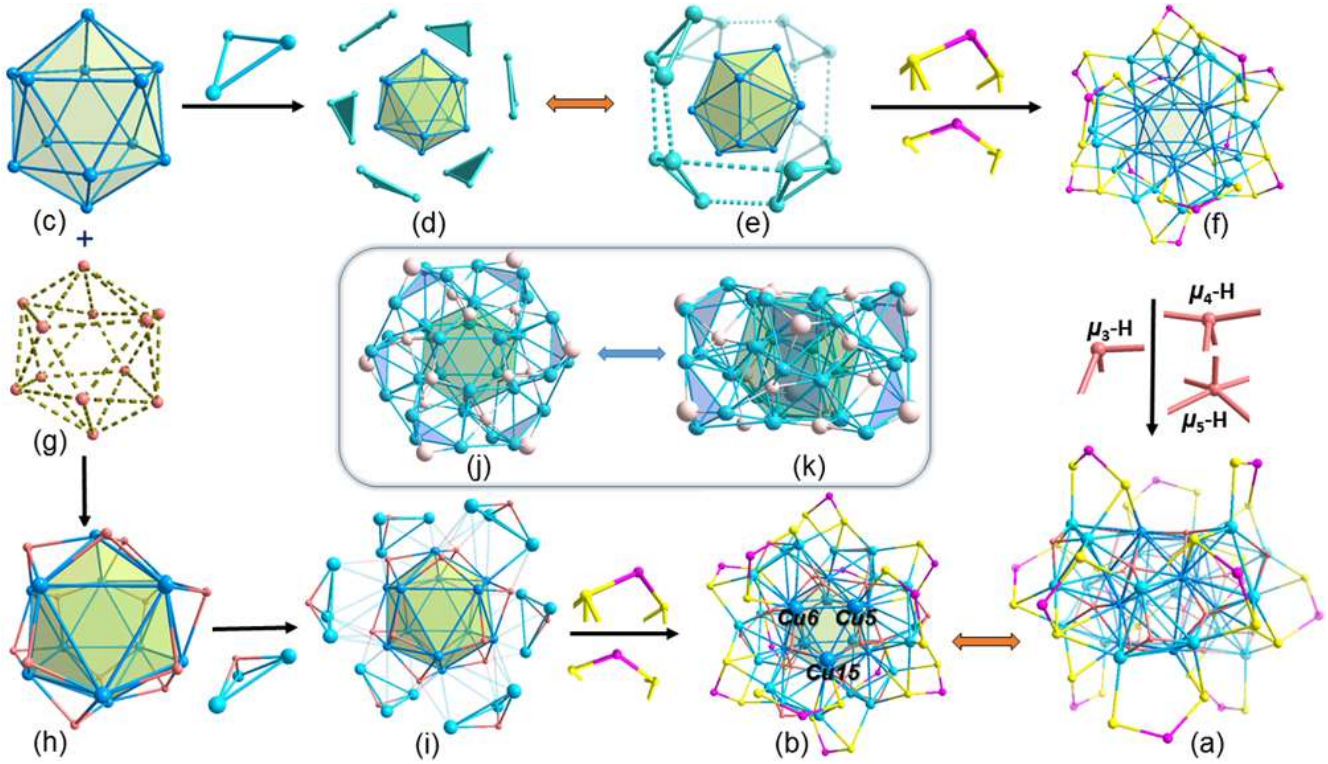

Figure 3. (a) Total structure of $[Cu_{30}H_{18}\{S_2P(O^nPr)_2\}_{12}]$ (**1H**) (side view); (b) Top view of **1H** where C_3 axis passes through Cu5-Cu6-Cu15 triangle (alkoxy groups in (a) and (b) are omitted for clarity); (c) The hollow Cu_{12} icosahedron; (d) Capping of six $[Cu_3]$ triangular motifs to the icosahedral Cu_{12} core; (e) Pseudorhombohedral architecture of Cu_{30} metal core in **1H** (f) Cu_{30} metal core with dtp ligand environment; (g) An icosahedral arrangement of twelve interstitial hydrides (6 μ_4 and 6 μ_5) around the Cu_{12} icosahedron; (h) Inner $Cu_{12}H_{12}$ framework; (i) $Cu_{30}H_{18}$ copper(I) polyhydride cage; (j, k) Top and side view of $Cu_{30}H_{18}$ cage in **1HN** (corresponding neutron diffraction of **1H**), respectively; color code: Cu_{ico} (blue) Cu_{cap} (cyan), H (light pink), P (pink), C (gray) and S (yellow).

metal (2.55 Å). In **1H**, the Cu_{ico}-Cu_{cap} distances between the atoms of the Cu_{12} icosahedron and the outer capping Cu atoms (range: 2.534(7)-2.896(6)) are slightly longer than the corresponding distances observed in $[Cu_{25}H_{22}(PPh_3)_{12}]Cl$ (range: 2.389(3)-2.604(3) Å).[38] *It is of note that the non-centered Cu_{12} icosahedral core in **1H** is similar to the M_{12} cores observed in Ag and Au clusters, for example $[Ag_{44}(p\text{-}MBA)_{30}]^{4-}$ [51] and $[Au_{32}(PPh_3)_8(dpa)_6]^{2-}$ (MBA = p-mercaptobenzoic acid, Hdpa = 2,2'-dipyridylamine),[52] showing for the first time that structurally alike NCs with inner empty M_{12} icosahedral core are isolable for all three coinage metals.*

The entire Cu_{30} metallic core in **1H** is wrapped by twelve dtp ligands. Half of them (three atop and three at the bottom) have axial orientation along the (vertical) C_3 axis, whereas the six other ligands coordinate in an equatorial fashion perpendicular to the C_3 axis (Figure 3a). These bidentate dtp ligands are coordinated to both capping and icosahedral copper atoms in various binding modes: the axial dtp ligands bind in a trimetallic triconnectivity fashion, while the equatorial dtp ligands prefer pentametallic pentaconnectivity pattern (Figure S8). The Cu-μ_2-S and Cu-μ_3-S distances are in the range of 2.329(1)-2.380(1) Å and 2.395(1)-2.795(1) Å, respectively. *As far as we know, the existence of a pentametallic pentaconnectivity binding pattern for the equatorial dtp ligands in **1H** is unique and hitherto unknown in the literature (Chart S1).*[54-56]

The presence of 18 hydrides was initially inferred by ^{1}H and ^{2}H NMR spectra of **1H** and **1D**, respectively followed by the X-ray structure determination of **1H**. However, their position remained uncertain until the results from single-crystal neutron diffraction analysis of **1HN**, the corresponding neutron structure of **1H,** were available (see supporting information for details). Within the $[Cu_{30}H_{18}]$ framework in **1HN** (Figure 3j and k) or **1H** (Figure 3g-i) out of the 20 triangular faces of the Cu_{12} icosahedron, six are capped by $[Cu_3]$ triangles, twelve are capped by interstitial hydrides (μ_4-H and μ_5-H in equal ratio) and two along the C_3 axis (top and bottom) remain uncapped. Each of the six outer $[Cu_3]$ triangles is capped by a μ_3 hydride. The observed Cu-μ_3-H distances in **1HN** range from 1.61(4) to 1.89(3) Å. Specific bond lengths of **1HN** are noted in Table 1. Interestingly, the twelve μ_4 and μ_5 hydrides surround the Cu_{12} icosahedron in such a way that they also form an icosahedral array (Figure 3g). Each μ_4-H is coordinated to three icosahedral copper atoms (one icosahedron face) and one of Cu_{cap} atom and occupies symmetrical positions around the C_3 axis. To our dismay, they favor a distorted seesaw geometry (average $<Cu_{cap}\text{-}H\text{-}Cu_{ico}$ = 159.7°) and can be fairly compared with the well-known molecule SF_4 with conventional seesaw geometry (<F-S-F = 173.1°). The Cu-μ_4-H distances in **1HN** range from 1.68(2) - 1.97(2) Å (avg. $d_{Cu\text{-}\mu4\text{-}H}$ = 1.81(2) Å). *To the best of our knowledge, hydrides with nearly seesaw coordination mode characterized by neutron diffraction is unprecedented* whereas

Table 1. Interatomic distances in Å (average and range) for $\mathbf{1_H}$ **-**$\mathbf{3_H}$ (X-ray), $\mathbf{1_{HN}}$ (neutron). Their respective DFT-computed values for models **1'** and **2'** are given in parenthesis. The ^{1}H NMR chemical shifts (in ppm) of hydrides for $\mathbf{1_H}$ **-**$\mathbf{3_H}$ are listed, together with their DFT-computed counterparts for **1'** and **2'** in parenthesis.

	$\mathbf{1_H}$	$\mathbf{1_{HN}}$ [b]	$\mathbf{2_H}$	$\mathbf{3_H}$
Cu_{ico}-Cu_{ico}	2.6581(7) (2.670) 2.5044(6)-2.9000(7) (2.570-2.923)	2.6400(1) 2.4714(1)-2.8061(1)	2.660 (3) (2.684) 2.493(3)-2.735(4) (2.579-2.937)	2.684(2) 2.5070(19)-2.7558(17)
Cu_{ico}-Cu_{cap}	2.6887(7) (2.657) 2.5338(7)-2.8961(6) (2.557-2.848)	2.6345(1) 2.4945(1)-2.7859(1)	2.619(4) (2.644) 2.449(4)-2.770(3) (2.563-2.792)	2.624(2) 2.479(2)-2.8011(18)
Cu_{cap}-Cu_{cap}	2.6070(7) (2.604) 2.5910(8)-2.6414(7) (2.595-2.619)	2.6313(1) 2.6241(1)-2.6426(1)	2.600(5) (2.715) 2.594(4)-2.614(5) (2.607-2.867)	2.605(3) 2.596(2)-2.626(3)
Cu-μ_3-H	1.68(6) (1.73) 1.62(7)-1.72(5) (1.71-1.74)	1.73(4) 1.61 (4)– 1.89(3)	1.78(2) (1.73) 1.77(1)-1.80(1) (1.71-1.74)	1.77(1) 1.77 -1.773(9)
Cu-μ_4-H	1.79(6) (1.83) 1.61(8)-2.12(7) (1.68-2.07)	1.81(2) 1.68(2) - 1.97(2)	1.80(2)[a] (1.83) 1.49(2)-1.90(9)[a] (1.68-2.08)	1.81(6)[a] 1.64(4)-2.10(7)[a]
Cu-μ_5-H	1.86(6) (1.87) 1.63(4)-2.08(6) (1.70-2.00)	1.81 (2) 1.68(2) - 1.97(2)	1.82(2)[b] (1.87) 1.49(2)-1.90(9)[b] (1.70-1.98)	1.85(2)[b] 1.64(8)-2.10(9)[b]
^{1}H NMR	3.52 (4.09), 0.78 (1.57), 0.60 (0.77)	-	3.14 (3.70), 0.57 (1.42), 0.27 (0.74)	3.09 , 0.54, 0.22

[a, b] The Cu-μ_4-H and Cu-μ_5-H distances were considered after removing two out of six Cu_3 triangular capping units associated with positional disorder (occupancy of each copper atoms are 0.667) in $\mathbf{2_H}$ and $\mathbf{3_H}$, respectively.

tetrahedral or near square-planar and trigonal pyramidal coordination modes of a four-coordinate hydride have been encountered before.[45,57] Each μ_5-H ($d_{avg.}$ = 1.83(2) Å) resides in a square pyramidal cavity formed by one icosahedron face and two Cu_{cap} atoms belonging to the same [Cu_3] units.

Over the past few years the nanocluster community has produced hundreds of atomically precise nanoparticles with well resolved structures. The mainstream of NCs is produced via wet chemical borohydride reductions and subsequently the desired species can be purified from the mixtures of products in most cases. On the other hand, a promising alternative method to yield molecularly pure new NCs is the ligand exchange method. In general, ligand exchange reactions lead to the modification of both the size and structure of the NC, but in exceptional cases it can retain both of them.[58] This is what happens when replacing the dtp ligands of $\mathbf{1_H}$ by their Se counterparts. The reaction of $\mathbf{1_H}$ with $NH_4[Se_2P(OR)_2]$ (R = ^{i}Pr and ^{i}Bu) afforded $[Cu_{30}H_{18}\{Se_2P(OR)_2\}_{12}]$ ($\mathbf{2_H}$: R = ^{i}Pr $\mathbf{3_H}$: R = ^{i}Bu) in 71 and 64 % yields (Scheme 1). These two compounds were characterized by using multinuclear (^{31}P{^{1}H}, ^{1}H and ^{2}H) NMR spectroscopy and single crystal XRD.

The ^{1}H NMR spectra of $\mathbf{2_H}$ and $\mathbf{3_H}$ show three sets of broad singlets ($\mathbf{2_H}$: 3.07, 0.51, 0.18 ppm and $\mathbf{3_H}$: 3.09, 0.54, 0.22 ppm) in equal intensities (Figure S9, S10). The observed upfield chemical shifts of hydrides in $\mathbf{2_H}$ and $\mathbf{3_H}$ are due to the higher polarizability of Cu-Se ($\mathbf{2_H}$ and $\mathbf{3_H}$) bonds, thus leading to more shielded hydrides in comparison to those in $\mathbf{1_H}$. Further, the ^{2}H NMR spectra of the deuteride analogoues of $\mathbf{2_H}$ and $\mathbf{3_H}$, $[Cu_{30}D_{18}\{S_2P(OR)_2\}_{12}]$ ($\mathbf{2_D}$**:** R = ^{i}Pr $\mathbf{3_D}$**:** R = ^{i}Bu), respectively show three sets of resonances which confirm the presence of three sets of hydrides (Figure S11, S12) in $\mathbf{2_H}$ and $\mathbf{3_H}$. The positive-ion ESI-MS spectra of $\mathbf{2_H}$ and $\mathbf{3_H}$ show prominent bands for the molecular ions $[\mathbf{2_H}]^{+2}$ and $[\mathbf{3_H}+Cu]^+$ at *m/z* 2804.39 (calcd. 2805.4), and *m/z* 6013.6 (calcd. 6013.2), respectively. Their corresponding simulated isotopic patterns are in line with the observed experimental ones (Figure S13, S14). Finally, the substitution of dtp ligands with diselenophosphates (dsep) was confirmed by ^{31}P{^{1}H} NMR spectroscopy. The ^{31}P{^{1}H} NMR spectra reveal the presence of two types of resonances for $\mathbf{2_H}$ (91.01 and 87.01 ppm) and for $\mathbf{3_H}$ (96.06 and 92.21 ppm) which are significantly shifted upfield in comparison with those observed in $\mathbf{1_H}$ (Figure S15, S16). Investigation of both ^{1}H(^{2}H) NMR spectra, ESI-MS (Figure S17, S18) and ^{31}P{^{1}H}, of $\mathbf{2_H}$ ($\mathbf{2_D}$) and $\mathbf{3_H}$ ($\mathbf{3_D}$) in comparison with $\mathbf{1_H}$ ($\mathbf{1_D}$) have predominantly suggested a sum of eighteen hydrides/deuterides and twelve diselenophosphate ligands, which are closely related through the C_3 axis in solution. Based on the above spectroscopic data for $\mathbf{2_H}$ and $\mathbf{3_H}$ which are produced *via* ligand replacement on $\mathbf{1_H}$, one can clearly deduce that geometry retention occurs in solution state. In $\mathbf{2_H}$, out of two resonances in ^{31}P{^{1}H} spectrum, the resonance at δ = 91.01 is flanked with one set of satellites and that at δ = 87.01 is flanked with two sets of satellites (Figure S15) which suggests two different types of dsep. Note that, the additional less intense peaks observed in both the ^{31}P{^{1}H} spectra of $\mathbf{2_H}$ and $\mathbf{3_H}$ are allied with the decomposition of the samples at ambient temperature in solution state. Several attempts to improve the spectra quality were unsucessful, even though single crystals were used for ^{31}P{^{1}H} NMR spectroscopy. Compounds $\mathbf{2_H}$ and $\mathbf{3_H}$ gradually decompose to diisopropylhydrogenphosphate, and diisobutylhydrogenphosphate respectively in their solution phase (Figure S19, S20). Given the solid state structure of $\mathbf{1_H}$ and the geometry retention

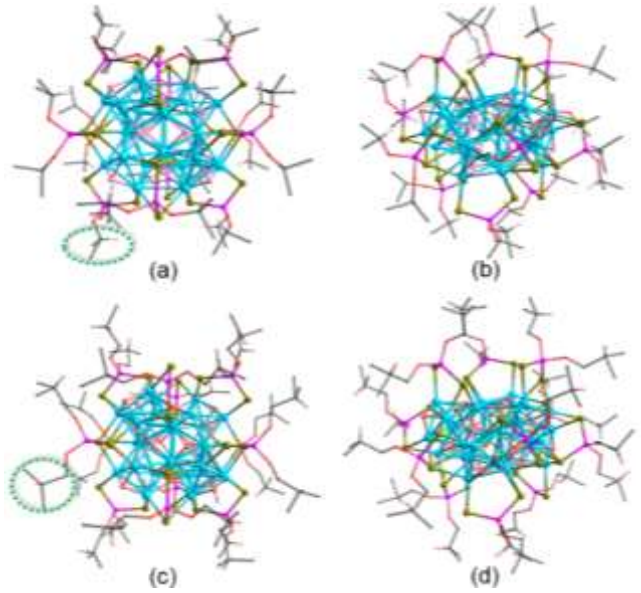

Figure 4. (a, b) Top and side view of solid state structure of **2H**. (c, d) Top and side view of solid state structure of **3H**. The dotted circles in (a) and (c) emphasize the different alkyl chains attached to **2H** and **3H.**

of **2H** in solution state, we suggest the observed chemical shift at lower frequency (δ = 86.3) in $^{31}P\{^{1}H\}$ NMR spectrum of **2H** can be ascribed to the six axial dsep ligand with the trimetallic triconnectivity bonding fashion.

As anticipated, the solid state structures of **2H** and **3H** (Figure 4, S21) unveil arrangements of 30 copper atoms, 18 hydrides and 12 diselenophosphate ligands with the same geometry as their parent cluster **1H**. The Cu_{ico}-Se distances in **2H** (avg. 2.571 Å) and in **3H** (avg. 2.554 Å) are slightly longer than the Cu_{cap}-Se (**2H**: avg. 2.543 Å) and (**3H** : avg. 2.539 Å) distances. Further, the observed Se···Se bite distances in **2H** (avg. 3.613 Å) and **3H** (avg. 3.632 Å) can be compared with those encountered in $[Cu_{20}(H)_{11}\{Se_2P(OR)_2\}_9]$ (R = ^{i}Pr and ^{t}Bu) (avg. 3.657 and 3.656 Å, respectively). The average Cu_{ico}-Cu_{ico} distance in **2H** (2.657(4) Å) is similar to that observed in its parent cluster **1H** (Cu_{ico}-Cu_{ico}: 2.658(7) Å) while in case of **3H** (2.684(2) Å) it is somewhat larger (Table 1). The Cu_{ico}-Cu_{cap} and Cu_{cap}-Cu_{cap} bond distances range from 2.448(4)-2.770(4) Å and 2.595(4)-2.613(7) in **2H** and (2.479(2)-2.801(2) Å and 2.596(2)-2.626(4) Å) in **3H**, respectively which are comparable to those encountered in **1H** (Table 1). The average Cu−μ_3-H, Cu−μ_4-H and Cu−μ_5-H distances in **2H** (1.68, 1.71 and 1.82 Å) and in **3H** (1.72, 1.70 and 1.83 Å), are similar to that encountered in **1H** (1.72, 1.70 and 1.83 Å) (Table 1). Clearly, both **2H** and **3H** retain the structural framework of **1H** with extreme precision. *To the best of our knowledge, the Se-donor stabilized clusters **2H** and **3H** synthesized via a ligand exchange method are the first structural evidences where the cluster shape and size are nearly unaffected upon complete ligand translation.*[59] *This is in stark contrast to the only existing Se-stabilized Cu_{20} cluster.*[47]

Density functional theory (DFT) calculations [60] were carried out on the simplified models $[Cu_{30}H_{18}\{E_2PH_2\}_{12}]$ (E = S: **1'**; E = Se: **2'**). Their optimized molecular structures were found to be of S_6 symmetry (see SI). They are consistent with the X-ray structures of **1H**, **2H** and **3H**, as exemplified by the relevant computed metrical data provided in Table 1. With respect to the hydride positions, the consistency with the neutron structure is particularly satisfying. No other hydride equilibrium position could be found. The computed ^{1}H NMR chemical shifts are in a qualitative agreement with the experimental ones (see Table 1) and there is a linear correlation between the two sets of values for both S and Se species, with a slope close to 1 (Figure S22). Such linear correlation is a general feature in this type of large polyhydrido copper clusters,[47,49] making DFT a useful tool for hydride localization when neutron data are not available. The copper natural atomic orbital (NAO) charges and the Cu···Cu Wiberg indices (Table 2) are typical of Cu(I) clusters.[47-50] The six less positively charged Cu(I) centers are those with the highest connectivity. The hydride NAO charges and the Cu-H Wiberg indices are also typical of Cu(I) polyhydrides. [47-50] As expected, the chalcogen charges indicate somewhat larger covalency in the case of Se, as compared to S. Both **1'** and **2'** exhibit substantial HOMO-LUMO gaps (1.75 and 1.71 eV at the BP86 level, respectively). The MO diagram of **1'** is given in Figure 5. The highest occupied levels are of large metal character and can be described as stemming from the 3d(Cu) block, with some ligand admixture. Among them, the five highest have substantial (~ 20%) hydride participation. The three lowest unoccupied orbitals have also substantial metal character.

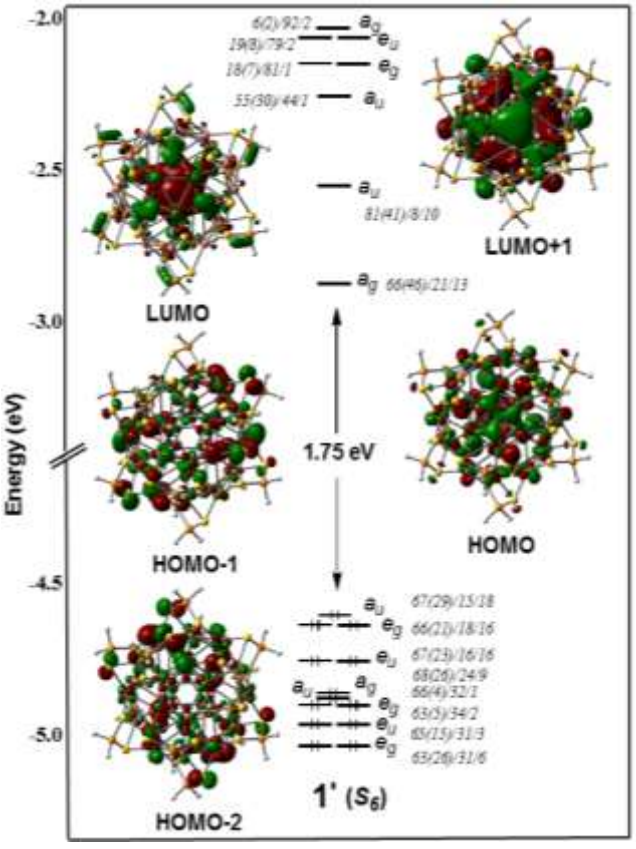

Figure 5. The Kohn-Sham MO diagram of **1'** with % localization given as: Cu_{30} (of which Cu_{12})/dtp_{12}/H_{18}.

The UV-vis spectrum of **1H** shows a major broad absorption band at 416 nm (Figure 6a), which is slightly blue-shifted with respect to its counterpart **2H** (λ_{max} = 432 nm). The time dependent density functional theory (TD-DFT)[60] simulated

spectrum (Figure 6a) of **1'** is in good agreement with its experimental counterpart (Figure 6a). The major transition associated with the low-energy band is computed at 406 nm and corresponds to a transition between the degenerate HOMO-1/HOMO-2 level of e_g symmetry to the LUMO+1 a_u orbital (Figure 5). The associated charge transfer is from the ligands (including the hydrides) to the inner Cu_{12} icosahedron. The corresponding transition computed for **2'** is found at 416 nm and is of a similar nature as that found for **1'**.

Table 2. Relevant computed NAO charges and Wiberg indices (range and average).

	1'	2'
Cu_{ico}	6 x 0.64 6 x 0.48	6 x 0.62 6 x 0.48
Cu_{cap}	6 x 0.48 18 x 0.63	6 x 0.48 12 x 0.60
μ_3-H	18 x 0.63	6 x 0.61
μ_4-H	-0.65	12 x 0.60
μ_5-H	-0.57	-0.65
E =S or Se (range)	-0.52	-0.58
Cu_{ico}-Cu_{ico}	-0.63/-0.69	-0.52
Cu_{ico}-Cu_{cap}	(0.038-0.072)	-0.48/-0.58
Cu_{cap}-Cu_{cap}	0.058	(0.037-0.069)
Cu-(μ_3-H)	(0.041-0.058)	0.056
Cu-(μ_4-H)	0.051	(0.046-0.060)
Cu-(μ_5-H)	(0.079-0.081)	0.053

The absorption spectra of $\mathbf{2_H}$ and $\mathbf{3_H}$ recorded in CH_2Cl_2 at 25 °C changed with time and decomposed within two days (Figure S23 and S24) while the absorption spectra of their parent cluster $\mathbf{1_H}$ retains its identity for 3 days in CH_2Cl_2 at 25 °C (Figure S7) indicating higher stability of the latter in solution state.

The thermal decomposition for the compound $\mathbf{2_H}$ was studied by thermogravimetric analysis (TGA) using the N_2 gas atmosphere which shows main thermal decomposition at the temperature range 150-200°C with weight loss of ~36 %, attributed to the elimination of hydrides, isopropyl substituents and phosphorous atoms present in the cluster (Figure 6b). The residual weight after the major decomposition produces the stable Cu-selenide complex ($Cu_{30}Se_{24-x}$), whereas the parent cluster, $\mathbf{1_H}$, shows the major decomposition at a slightly higher temperature range 180-250 °C in comparison to $\mathbf{2_H}$ with similar weight loss (Figure 6b).

Owing to their synergetic and enhanced catalytic,[61-65] optical,[66-70] and electrochemical[71-74] development, alloy NCs have recently outpaced that of their homometallic counterparts. Unlike Au and Ag, Cu has realized fewer accomplishments as a host metal for the generation of alloy NCs. Very recently, we reported the first and still unique structurally-precise Cu-M (M = group 10 element) bimetallic NC, namely $[PdH_2Cu_{14}\{S_2P(O^iPr)_2\}_6(C{\equiv}CPh)_6]$.[75] It was synthesized by the reaction of a polyhydrido copper cluster ($[Cu_{20}H_{11}\{S_2P(O^iPr)_2\}_9]$ or $[Cu_{32}H_{20}\{S_2P(O^iPr)_2\}_{12}]$) with Pd(II) in the presence of alkynes. We were thus tempted to react $\mathbf{1_H}$ with Pd(II) in the presence of phenyl acetylene as an auxiliary ligand. The reaction leads to the isolation of the new cluster $[PdH_2Cu_{14}\{S_2P(O^nPr)_2\}_6(C{\equiv}CPh)_6]$ (**4**) (Scheme 1). We also synthesized the fluorinated derivative $[PdH_2Cu_{14}\{S_2P(O^nPr)_2\}_6(C{\equiv}CC_6H_4F)_6]$ (**5**) by introducing the $HC{\equiv}CC_6H_4F$ alkyne. Clusters **4** and **5** have been fully characterized by multinuclear NMR spectroscopy, ESI-mass spectrometry and single crystal X-ray diffraction.

The $^{31}P\{^1H\}$ NMR spectrum of **4** and **5** exhibits single resonance at 106.7 and 106.2 ppm, respectively (Figure S25, S26). The ^1H NMR spectra of both clusters **4** and **5** show the characteristic signals corresponding to dithiophosphates (Figures S27, S28). In addition, each spectrum shows a broad singlet hydride resonance at 0.46, and 0.33 ppm for **4** and **5**, respectively. The positive-ion ESI mass spectra of **4** and **5** clearly display prominent bands attributed to their respective molecular ions $[\mathbf{4}]^+$ at *m/z* 2882.8 (calcd. 2883.3), and $[\mathbf{5}+H]^+$ at *m/z* 2991.3 (calcd. 2990.2). Their respective theoretical isotopic patterns are in good agreement with the experimental ones (Figure S29, S30).

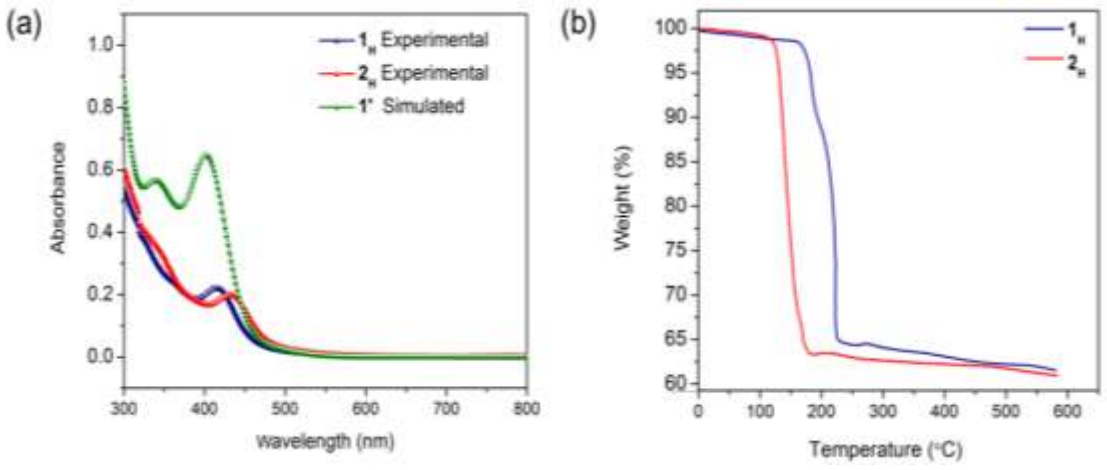

Figure 6. (a) UV–vis spectrum of $\mathbf{1_H}$ and $\mathbf{2_H}$ in 1 x 10^{-5} M CH_2Cl_2 at room temperature. (b) TGA of $\mathbf{1_H}$ and $\mathbf{2_H}$.

The coordination of alkynes adopting a μ_3:η^1, η^1, η^2 pattern to Cu metals in clusters **4** and **5** was monitored initially by a ^{13}C NMR spectroscopy. The $^{13}C\{^1H\}$ NMR spectra showed two signals corresponding to carbon atoms of alkyne for **4** (δ = 127.5 and 90.5 ppm) and for **5** (δ = 126.0 and 91.9 ppm) (Figure S31, S32) whereas free phenyl acetylene and 3-fluoro phenyl acetylene moieties show signals at δ = 81.4 and 82.3, respectively. This indicates the true coordination of alkynes within **4** and **5**. Out of two signals for each clusters the quaternary carbons in **4** and **5** can be assigned to the less intense peaks at δ = 90.5 and 91.9 ppm in **4** and **5**, respectively. Furthermore, the bonding of alkynes to the Cu metals in **4** and **5** were supported by FT-IR spectra. The results showed a weak and broad band at 1990 cm^{-1} corresponding to $\nu_{C\equiv C}$ in **4** which is about 120 cm^{-1} lower than the observed value for free phenyl acetylene (2110 cm^{-1}) (Figure S33). The respective $\nu_{C\equiv C}$ frequency in **5** was also occurred at similar position (Figure S34).

The X-ray structures of **4** and **5** are consistent with all the spectroscopic assignments (Figure 7). They exhibit a Pd-centered bi-capped icosahedron ($PdH_2@Cu_{14}$) co-protected by 6 dtp and 6 alkynyl ligands. In addition, two hydrides bonded to Pd are embodied in the icosahedron. The metallic frameworks of **4** and **5** have idealized D_{3d} symmetry, where the C_3 passes through the two capping Cu atoms, the two hydrides and the central Pd atom. Their overall geometry is similar to our recently reported cluster $[PdH_2Cu_{14}\{S_2P(O^iPr)_2\}_6(C\equiv CPh)_6]$[75] (Figure 7a-c). One of the noteworthy features in **4** and **5** is that the central Pd(0) atom is connected to the two hydrides and twelve Cu atoms, thus reaching a coordination number of 14, the highest so far documented.

Unsurprisingly, DFT calculations indicate that **4** and **5** have the same electronic structure as their isostructural relative $[PdH_2Cu_{14}\{S_2P(O^iPr)_2\}_6(C\equiv CPh)_6]$.[75] They can be described as made of a linear 14-electron $[PdH_2]^{2-}$ complex encapsulated in a bicapped icosahedron made of 14 Cu(I) centers, the resulting $[(PdH_2)@Cu_{14}]^{12+}$ core being further stabilized by 6 dtp and 6 alkynyl anionic ligands.

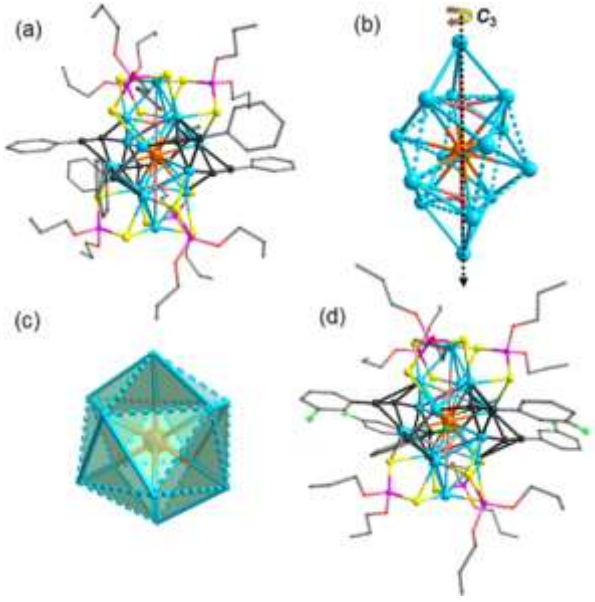

Figure 7. (a, d) Total structures of **4** and **5,** respectively (hydrogen atoms are removed for clarity). (b) A $PdCu_{14}$ metal core frame work in **4**. (c) A Pd-centred Cu_{12} icosahedron in **4**. Color code: Cu (cyan), S (yellow), P (pink), O (red), F (green), and H (light Pink).

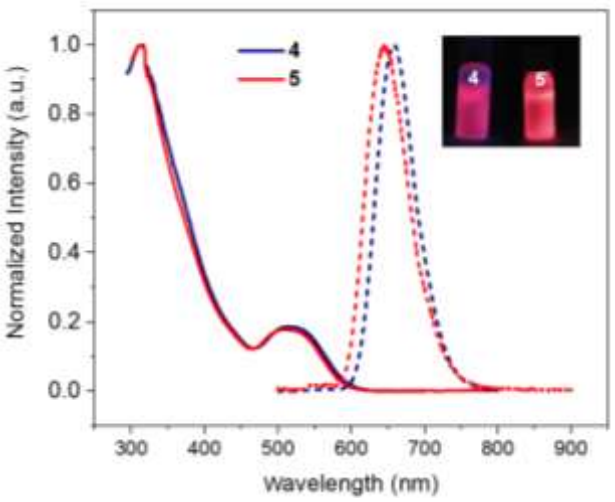

Figure 8. UV-Vis (solid lines) and emission (dashed lines) spectra of **4** and **5**.

Both clusters **4** and **5** are red in color with a marginal variance to the naked eye. The UV-Vis spectrum of **4** and **5** shows a broad absorption band around 495-540 nm with nearly the same intensity. The absorption spectrum of **4** recorded in CH_2Cl_2 at 25 °C changed with time and completely decomposed within 10 days (Figure S35), while **5** sustains its identity for 5 days (Figure S36). However, the time-dependent UV-Vis spectra of **4** and **5** remain unchanged for months when the powders or crystalline forms of **4** and **5** dissolve in CH_2Cl_2 to obtain the spectra each time; indicating their high stability in solid-state. Both clusters **4** and **5** are luminescent in their solid and solution state at cryogenic temperature. The emission spectrum of **4** features a maximum at 659 nm in 2-methyl tetrahydrofuran at 77K, whereas the emission maximum occurs at 644 nm for **5**, which is a blue-shift compared to **4** (Figure 8, S37).

Conclusion

In summary, this work describes the synthesis and structural characterization of a polyhydrido Cu(I) cluster $[Cu_{30}H_{18}\{S_2P(O^nPr)_2\}_{12}]$, $\mathbf{1_H}$ which is the first example embodying a non-centered Cu_{12} icosahedron. This hollow icosahedron is capped by six $[Cu_3]$ triangles, resulting in a Cu_{30} core of ideal S_6 symmetry. Six among the twelve surface dtp ligands show a unique binding mode of pentametallic pentaconnectivity, hitherto unknown in the literature. Furthermore, two new Se-protected Cu_{30} clusters $[Cu_{30}H_{18}\{Se_2P(OR)_2\}_{12}]$, $\mathbf{2_H}$ (R = ^{i}Pr) and $\mathbf{3_H}$ (R = ^{i}Bu), have been isolated via a ligand exchange protocol from $\mathbf{1_H}$. Their X-ray structures reveal strict conservation of cluster structure and size upon ligand exchange. This methodology is predominantly beneficial for the Se-donor stabilizing ligands, which readily decomposes in solution in the presence of reducing reagents. In addition, two new Pd-Cu alloys containing Pd(0) have been synthesized by using $\mathbf{1_H}$ as a synthon, which show photoluminescence in both solid and solution states at 77K. We anticipate that the isolation of this novel hollow icosahedral (Cu_{12}) based NCs in their pure forms will become new templates for the synthesis of various alloy clusters with enhanced synergistic properties for multiple potential applications.

Acknowledgements

This work was supported by the Ministry of Science and Technology in Taiwan (MOST 106-2113-M-259-010; 108-2923-M-259-001) and the France-Taiwan ANR-MOST 2018 program (project Nanoalloys). The GENCI is acknowledged for HPC resources (Project A0050807367). We thank Dr. A. Y. Kovalevsky (Neutron Scattering Division, ORNL) for his help with X-ray data collection. This research used resources at the Spallation Neutron Source, a DOE Office of Science User Facility operated by the Oak Ridge National Laboratory, under Contract No. DE-AC05-00OR22725 with UT-Battelle, LLC.

Keywords: Copper • nanocluster • hollow icosahedron • hydride •neutron diffraction • ligand exchange• palladium

[1] H. Müller, A. J. Bradley, *J. Chem. Soc.* **1926**, 1669-1673.
[2] A. Wurtz, *Ann. Chim. Phys.* **1844**, *11*, 250-252.
[3] S. A. Bezman, M. R. Churchill, J. A. Osborn, J. Wormald, *J. Am. Chem. Soc.* **1971**, *93*, 2063-2065.
[4] T. H. Lemmen, K. Folting, J. C. Huffman, K. G. Caulton, *J. Am. Chem. Soc.* **1985**, *107*, 7774-7775.
[5] C. F. Albert, P. C. Healy, J. D. Kildea, C. L. Raston, B. W. Skelton, A. H. White, *Inorg. Chem.* **1989**, *28*, 1300-1306.
[6] T. Saito, T. Yokozawa, T. Ishizaki, T. Moroi, N. Sayo, T. Miura, H. Kumobayashi, *Adv. Synth. Catal.* **2001**, *343*, 264-267.
[7] N. P. Mankad, D. S. Laitar, J. P. Sadighi, *Organometallics* **2004**, *23*, 3369-3371.
[8] Y. Takemura, T. Nakajima, T. Tanase, M. Usuki, H. Takenaka, E. Goto, M. Mikuriya, *Chem. Commun*. **2009**, 1664-1666.
[9] Y. Takemura, T. Nakajima, T. Tanase, *Dalton Trans.* **2009**, 10231-10243.
[10] G. D. Frey, B. Donnadieu, M. Soleilhavoup, G. Bertrand, *Chem. Asian J.* **2011**, *6*, 402-405.
[11] J. Li, J. M. White, R. J. Mulder, G. E. Reid, P. S. Donnelly, R. A. J. O'Hair, *Inorg. Chem.* **2016**, *55*, 9858-9868.
[12] K. Nakamae, M. Tanaka, B. Kure, T. Nakajima, Y. Ura, T. A. Tanase, *Chem.- Eur. J.* **2017**, *23*, 9457-9461.
[13] H. Z. Ma, J. Li, A. J. Canty, R. A. J. O'Hair, *Dalton Trans*. **2017**, *46*, 14995-15003.
[14] T. Nakajima, Y. Kamiryo, K. Hachiken, K. Nakamae, Y. Ura, T. Tanase, *Inorg. Chem*. **2018**, *57*, 11005-11018.
[15] A. Dedieu, in *Transition Metal Hydrides*; Wiley-VCH: Weinheim, Germany, 1992.
[16] R. Poli, M. Peruzzini, in *Recent Advances in Hydride Chemistry*; Elsevier: Amsterdam, 2001; pp 557-578.
[17] R. S. Dhayal, W. E. van Zyl, C. W. Liu, *Acc. Chem. Res*. **2016**, *49*, 86-95.
[18] R. H. Crabtree, *in Encyclopedia of Inorganic Chemistry*, 2nd ed.; (Eds.: R. B. King) Wiley: Chichester, U.K., **2005**; Chapter 8, pp 1.
[19] K. Yvon, G. Renaudin, *in Encyclopedia of Inorganic Chemistry*, 2nd ed.; (Eds.: R. B. King) Wiley: Chichester, U.K., 2005; Vol. 3, p 1814.
[20] S. K. Brayshaw, M. J. Ingleson, J. C. Green, J. S. McIndoe, P. R. Raithby, G. Kociok-Köhn, A. S. Weller, *J. Am. Chem. Soc.* **2006**, *128*, 6247-6263.
[21] D. Zhao, D. Yuan, H.-C. Zhou, *Energy Environ. Sci.* **2008**, *1*, 222-235.
[22] J. Graetz, *Chem. Soc. Rev.* **2009**, *38*, 73-82.
[23] J. Yang, A. Sudik, C. Wolverton, D. Siegel, *J. Chem. Soc. Rev.* **2010**, *39*, 656-675.
[24] B. Cornils, W. A. Herrmann, in *Applied Homogeneous Catalysis with Organometallic Compounds*; Wiley-VCH: Weinheim, Germany, **1996**.
[25] S. Gaillard, J.-L. Renaud, *ChemSusChem* **2008**, *1*, 505-509.
[26] D. H. Appella, Y. Moritani, R. Shintani, E. M. Ferreira, S. L. Buchwald, *J. Am. Chem. Soc.* **1999**, *121,* 9473-9474.
[27] H. Brunner, W. Miehlng, *J. Organomet. Chem*. **1984**, *275*, c17-c21.
[28] H. D. Kaesz, R. B. Saillant, *Chem. Rev.* **1972**, *72*, 231-281.
[29] Z. Lin, M. B. Hall, *Coord. Chem. Rev.* **1994**, *135*, 845-879.
[30] S. Sabo-Etienne, B. Chaudret, *Coord. Chem. Rev.* **1998**, *178*, 381-407.
[31] R. S. Dhayal, W. E. van Zyl, C. W. Liu, *Dalton Trans.* **2019**, *48,* 3531-3538.
[32] B.-H. Lee, C.-C. Wu, X. Fang, C. W. Liu, J.-L. Zhu, *Catal Lett.* **2013**, *143*, 572-577.
[33] Q. Tang, Y. Lee, D.-Y. Li, W. Choi, C. W. Liu, D. Lee, D.-e. Jiang, *J. Am. Chem. Soc*. **2017**, *139*, 9728-9736.
[34] A. W. Cook, Z. R. Jones, G. Wu, S. L. Scott, T. W. Hayton, *J. Am. Chem. Soc.* **2018**, *140*, 394-400.
[35] A. W. Cook, T. W. Hayton, *Acc. Chem. Res.* **2018**, *51*, 2456-2464.
[36] T. Nakajima, Y. Kamiryo, M. Kishimoto, K. Imai, K. Nakamae, Y. Ura, T. Tanase, *J. Am. Chem. Soc.* **2019**, *141*, 8732-8736.
[37] C. Sun, N. Mammen, S. Kaappa, P. Yuan, G. Deng, C. Zhao, J. Yan, S. Malola, K. Honkala, H. Häkkinen, B. K. Teo, N. Zheng, *ACS Nano* **2019**, *135*, 5975-5986.
[38] T.-A. D. Nguyen, Z. R. Jones, B. R. Goldsmith, W. R. Buratto, G. Wu, S. L. Scott, T. W. Hayton, *J. Am. Chem. Soc.* **2015**, *137*, 13319-13324.
[39] K. K. Chakrahari, J.-H. Liao, S. Kahlal, Y.-C. Liu, M.-H. Chiang, J.-Y. Saillard, C. W. Liu, *Angew. Chem.* **2016**,*128*,14924-14928; *Angew. Chem. Int. Ed.* **2016**, *55*, 14704-14708.
[40] K. K. Chakrahari, R. P. B. Silalahi, J.-H. Liao, S. Kahlal, Y.-C. Liu, J.-F. Lee, M.-H. Chiang, J.-Y. Saillard, C. W. Liu, *Chem. Sci*. **2018**, *9*, 6785-6795.
[41] A. Ghosh, R.-W. Huang, B. Alamer, E. Abou-Hamad, M. N. Hedhili, O. F. Mohammed, O. M. Bakr, *ACS Materials Lett.* **2019**, *1*, 297-302.
[42] C. W. Liu, B. Sarkar, Y.-J. Huang, P.-K. Liao, J.-C. Wang, J.-Y. Saillard, S. Kahal, *J. Am. Chem. Soc.* **2009**, *131*, 11222-11233.
[43] P.-K. Liao, B. Sarkar, H.-W. Chang, J.-C. Wang, C. W. Liu, *Inorg. Chem.* **2009**, *48*, 4089-4097.
[44] P.-K. Liao, K.-G. Liu, C.-S. Fang, C. W. Liu, J. P. Jr. Fackler, Y.-Y. Wu, *Inorg. Chem.* **2011**, *50*, 8410-8417.
[45] P.-K. Liao, C.-S. Fang, A.-J. Edwards, S. Kahlal, J.-Y. Saillard, C. W. Liu, *Inorg. Chem.* **2012**, *51*, 6577-6591.
[46] R. S. Dhayal, J.-H. Liao, Y.-R. Lin, P.-K. Liao, S. Kahlal, J.-Y. Saillard, C. W. Liu, *J. Am. Chem. Soc*. **2013**, *135*, 4704-4707.
[47] R. S. Dhayal, J.-H. Liao, X. Wang, Y.-C. Liu, M.-H. Chiang, S. Kahlal, J.-Y. Saillard, C. W. Liu, *Angew. Chem.* **2015**, *127*, 13808-13812; *Angew. Chem. Int. Ed.* **2015**, *54*, 13604-13608.
[48] A. J. Edwards, R. S. Dhayal, P.-K. Liao, J.-H. Liao, M.-H. Chiang, R. O. Piltz, S. Kahlal, J.-Y. Saillard, C. W. Liu, *Angew. Chem*. 126, 7342-7346; *Angew. Chem. Int. Ed.* **2014**, *53*, 7214-7218.
[49] R. S. Dhayal, J.-H. Liao, S. Kahlal, X. Wang, Y.-C. Liu, M.-H. Chiang, W. E. van Zyl, J.-Y. Saillard, C. W. Liu, *Chem. Eur. J.* **2015**, *21*, 8369-8374.
[50] R. S. Dhayl, H.-P. Chen, J.-H. Liao, W. E. van Zyl, C. W. Liu, *ChemistrySelect* **2018**, *3,* 3603-3610.
[51] A. Desireddy, B. C. Conn, J. Guo, B. Yoon, R. N. Barnett, B. N. Monahan, K. Kirschbaum, W. P. Griffith, R. L. Whetten, U. Andmann, T. P. Bigioni, *Nature* **2013**, *501*, 399-402.
[52] S.-F. Yuan, C.-Q. Xu, J. Li, Q.-M. Wang, *Angew. Chem.* **2019**,*131, 5967-5970; Angew. Chem. Int. Ed*. **2019**, *58*, 1-5.
[53] P. Yuan, R. Chen, X. Zhang, F. Chen, J. Yan, C. Sun, D. Ou, J. Peng, S. Lin, Z. Tang, B. K. Teo, L.-S. Zheng, N. Zheng *Angew. Chem.* **2018**,*131, 845-849; Angew. Chem. Int. Ed*. **2018**, *58*, 835-839.
[54] I. Haiduc, D. B. Sowerby, S.-F. Lu, *Polyhedron* **1995**, *14*, 3389-3472.
[55] I. Haiduc, L. Y. Goh, *Coord. Chem. Rev.* **2002**, *224*, 151-170.
[56] T. S. Lobana, J.-C. Wang, C. W. Liu, *Coord. Chem. Rev.* **2007**, *251*, 91-110.
[57] R. P. B. Silalahi, G.-R. Huang, J.-H. Liao, T.-H. Chiu, K. K. Chakrahari, X. Wang, J. Cartron, S. Kahlal, J.-Y. Saillard, C. W. Liu, *Inorg. Chem*. **2020**, *59*, 2536-2547.
[58] L. G. AbdulHalim, N. Kothalawala, L. Sinatra, A. Dass, O. M. Bakr, *J. Am. Chem. Soc.* **2014**, *136*, 15865-15868.
[59] X. Kang, M. Zhu, *Small* **2019**, 1902703.
[60] See Computaional details in supporting information.
[61] R. P. B. Silalahi, K. K. Chakrahari, J.-H. Liao, S. Kahlal, Y.-C. Liu, M.-H. Chiang, J.-Y. Saillard, C. W. Liu, *Chem. Asian J.* **2018**, *13*, 500-504.

[62] M. S. Bootharaju, C. P. Joshi, M. R. Parida, O. F. Mohammed, O. M. Bakr, *Angew. Chem.* **2016**, *128,* 934-938; *Angew. Chem. Int. Ed.* **2016**, *55*, 922-926.

[63] Z. Lei, X.-Y. Pei, Z.-G. Jiang, Q.-M. Wang, *Angew. Chem.* **2014**, *126*, 12985-12989; *Angew. Chem. Int. Ed*. **2014**, *53*, 12771-12775.

[64] S. Wang, X. Meng, A. Das, T. Li, Y. Song, T. Cao, X. Zhu, M. Zhu, R. Jin, *Angew. Chem.* **2014**, *126*, 2408-2412; *Angew. Chem. Int. Ed*. **2014**, *53*, 2376-2380.

[65] T. Udayabhaskararao, Y. Sun, N. Goswami, S. K. Pal, K. Balasubramanian, T. Pradeep, *Angew. Chem.* **2012**, *124*, 2197; *Angew. Chem. Int. Ed.* **2012**, *51*, 2155-2159.

[66] H. Qian, D.-e. Jiang, G. Li, C. Gayathri, A. Das, R. R. Gil, R. Jin, *J. Am. Chem. Soc*. **2012**, *134*, 16159-16162.

[67] Y. Liu, X. Chai, X. Cai, M. Chen, R. Jin, W. Ding, Y. Zhu, *Angew. Chem.* **2018**, *130*, 9923-9927; *Angew. Chem. Int. Ed.* **2018**, *57*, 9775-9779.

[68] C. Yao, J. Chen, M.-B. Li, L. Liu, J. Yang, Z. Wu, *Nano Lett.* **2015**, *15*, 1281-1287.

[69] S. Wang, S. Jin, S. Yang, S. Chen, Y. Song. J. Zhang, M. Zhu, *Sci. Adv.* **2015**, *1: e1500441*.

[70] S. Xie, H. Tsunoyama, W. Kurashige, Y. Negishi, T. Tsukuda, *ACS Catal.* **2012**, *2*, 1519-1523.

[71] C. A. Fields-Zinna, M. C. Crowe, A. Dass, J. E. F. Weaver, R. W. Murray, *Langmuir* **2009**, *25*, 7704-7710.

[72] K. Kwak, Q. Tang, M. Kim, D.-e. Jiang, D. Lee, *J. Am. Chem. Soc*. **2015**, *137,* 10833-10840.

[73] L. Liao, S. Zhou, Y. Dai, L. Liu, C. Yao, C. Fu, J. Yang, Z. Wu, *J. Am. Chem. Soc.* **2015**, *137*, 9511-9514.

[74] J.-P. Choi, C. A. Fields-Zinna, R. L. Stiles, R. Balasubramanian, A. D. Douglas, M. C. Crowe, R. W. Murray, *J. Phys. Chem. C* **2010**, *114*, 15890-15896.

[75] K. K. Chakrahari, R. P. B. Silalahi, T.-H. Chiu, X. Wang, N. Azrou, S. Kahlal, Y.-C. Liu, M.-H. Chiang, J.-Y. Saillard, C. W. Liu, *Angew. Chem.* **2019**, *131*, 4997-5001; *Angew. Chem. Int. Ed*. **2019**, *58*, 4943-4947.

10.1002/chem.202001449

WILEY-VCH

Entry for the Table of Contents

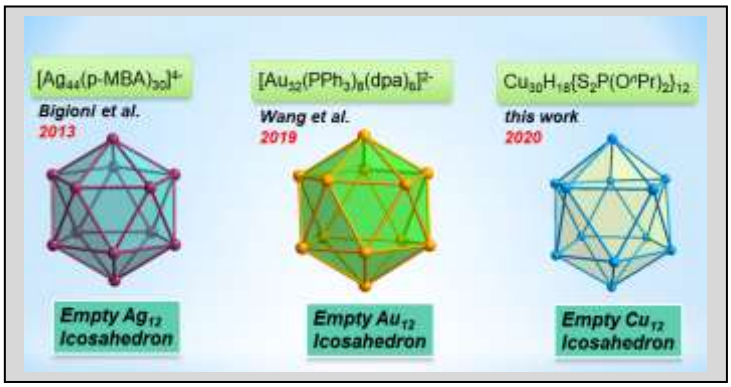

Atomically and structurally precise polyhydrido copper nanocluster $[Cu_{30}H_{18}\{S_2P(O^nPr)_2\}_{12}]$ which embodied an unprecedented inner hollow Cu_{12} icosahedron core has been isolated and fully characterized by single-crystal neutron diffraction analysis; while existence of Ag_{12} and Au_{12} icosahedra have reported in the year 2013 and 2019, respectively.

***E-mail:** chenwei@mail.ndhu.edu.tw. (ORCID iD- C. W. Liu: 0000-0003-0801-6499)